

Abstract

Nitrogen-fixing (N₂) cyanobacteria provide bioavailable nitrogen to vast ocean regions but are in turn limited by iron (Fe) and/or phosphorus (P), which may force them to employ alternative nitrogen acquisition strategies. The adaptive responses of nitrogen-fixers to global-change drivers under nutrient-limited conditions could profoundly alter the current ocean nitrogen and carbon cycles. Here, we show that the globally-important N₂-fixer *Trichodesmium* fundamentally shifts nitrogen metabolism towards organic-nitrogen scavenging following long-term high-CO₂ adaptation under iron and/or phosphorus (co)-limitation. Global shifts in transcripts and proteins under high CO₂/Fe-limited and/or P-limited conditions include decreases in the N₂-fixing nitrogenase enzyme, coupled with major increases in enzymes that oxidize trimethylamine (TMA). TMA is an abundant, biogeochemically-important organic nitrogen compound that supports rapid *Trichodesmium* growth while inhibiting N₂ fixation. In a future high-CO₂ ocean, this whole-cell energetic reallocation towards organic nitrogen scavenging and away from N₂-fixation may reduce new-nitrogen inputs by *Trichodesmium*, while simultaneously depleting the scarce fixed-nitrogen supplies of nitrogen-limited open ocean ecosystems.

Importance

Trichodesmium is among the most biogeochemically-significant microorganisms in the ocean, since it supplies up to 50% of the new nitrogen supporting open ocean food webs. We used *Trichodesmium* cultures adapted to high CO₂ for 7 years followed by additional exposure to iron and/or phosphorus (co)-limitation. We show that ‘future ocean’ conditions of high CO₂ and concurrent nutrient limitation(s) fundamentally shift nitrogen metabolism away from nitrogen fixation, and instead towards upregulation of organic-nitrogen scavenging pathways. We show that *Trichodesmium*’s responses to projected future ocean conditions include decreases in the nitrogen-fixing nitrogenase enzymes, coupled with major increases in enzymes that oxidize the abundant organic nitrogen source trimethylamine (TMA). Such a shift towards organic nitrogen uptake and away from nitrogen fixation may substantially reduce new-nitrogen inputs by *Trichodesmium* to the rest of the microbial community in the future high-CO₂ ocean, with potential global implications for ocean carbon and nitrogen cycling.

Keywords: nutrient co-limitation, nitrogen fixation, *Trichodesmium*, global change, ocean acidification, microbial ecology, cyanobacteria, evolution, TMA, trimethylamine

68 Introduction

69 Oceanic food webs and climate feedbacks are significantly influenced by carbon dioxide (CO₂)
70 and nitrogen (N₂) fixing microbes, thereby contributing to both global productivity and
71 biogeochemistry (1-3) . However, only a handful of studies have investigated the physiological
72 and evolutionary responses of the globally important, photoautotrophic, N₂-fixing,
73 cyanobacterium *Trichodesmium erythraeum* strain IMS101 to high CO₂ under multiple limiting
74 nutrient regimes (4-6). Simultaneous iron (Fe) and phosphorus (P) co-limitation of IMS101 under
75 both low and high CO₂ has been found to yield higher growth rates, reduced cell sizes, and a
76 unique Fe/P protein complement, as compared to single limitation by either Fe or P alone (5, 7).
77 This fitness advantage conferred by Fe/P ‘balanced limitation’ contrasts with the long-standing
78 Liebig limitation model (8) and has implications for global biogeochemical cycles in both the
79 current and future ocean (3).

80 Oligotrophic populations are predicted to potentially experience longer periods of
81 enhanced nutrient (co)-limitation due to intensifying Fe-stress under high CO₂ (5, 9) and reduced
82 vertical P supplies from increased density-driven stratification (3, 10). However, a major
83 unknown is the potential change to future new nitrogen inputs by globally distributed N₂-fixing
84 microbes (diazotrophs). Indeed, past research has demonstrated significant decreases in growth
85 and N₂ fixation of marine diazotrophs under Fe-limitation, with molecular evidence indicating
86 iron reallocation via reduction in the photosystem I to photosystem II (PSI:PSII) ratio, decreases
87 in metalloenzyme inventories, and increases in Fe-stress PS antennae abundances (5, 11-13).
88 Additionally, *Trichodesmium* has been demonstrated to take up both inorganic (e.g. nitrate and
89 ammonia) and organic (e.g. amino acids) nitrogen species, thereby inhibiting N₂ fixation(14, 15).
90 However, because much of the low-latitude surface ocean is largely nitrogen limited (16), fixed

91 N sources can be severely depleted, resulting in a marked dependence on Fe and P bioavailability
92 to fuel N₂ fixation (1, 3).

93 To date, nearly all diazotrophic nitrogen assimilation research has focused on the
94 relationship between N₂ fixation and nitrate, ammonia, and amino acid uptake, resulting in the
95 view that ammonia is the preferred microbial nitrogen source for both diazotrophic and non-
96 diazotrophic microbes (17). Identifying and measuring preferentially scavenged organic nitrogen
97 species by marine microbes has been largely precluded by rapid biochemical turnover *in situ*.
98 Furthermore, microbial consortia aggregating around microbial species of interest can also
99 inhibit discernment between microbial uptake of specific substrates (18).

100 In this study, functional genomics and molecular physiology provide strong evidence that
101 following adaptation to high CO₂, *Trichodesmium* allocates the greatest biosynthetic investment
102 into the acquisition of the organic nitrogen substrate trimethylamine (TMA), and potentially
103 other organic nitrogen- and sulfur-containing compounds. This shift in nitrogen acquisition
104 pathways under high-CO₂ conditions is predicted to be mediated by large increases in bacterial
105 flavin-containing monooxygenase (FMO) coupled to global shifts in transcription and
106 translation. This indicates both a fundamental change in nitrogen and global cellular strategy,
107 whereby iron-rich biosynthetic pathways including N₂ fixation and photosynthesis are
108 significantly reduced under Fe-limited, high-CO₂ conditions, in parallel with increased
109 biosynthesis of the predicted TMA-oxidizing FMO enzyme. Additionally, N₂ fixation is
110 inhibited in the presence of exogenous TMA in a manner similar to that seen with nitrate and
111 ammonia, with TMA simultaneously supporting growth rates equivalent to those seen while
112 fixing N₂. Methylated amine compounds like TMA are products of protein putrefaction and
113 degradation of quaternary amine osmoregulators (e.g. glycine betaine)(19) and are thus

114 ubiquitous in the marine environment, representing a considerable pool of C and N with reported
115 standing concentrations in the nano- to micromolar range (20, 21). Hence, future CO₂ levels and
116 limiting Fe may exacerbate cellular Fe-stress, resulting in a fundamental metabolic shift whereby
117 *Trichodesmium* reallocates resources away from N₂ fixation and towards FMO-mediated organic
118 nitrogen scavenging. The resulting metabolism change observed in *Trichodesmium* necessitates a
119 reassessment of the relationship between new nitrogen inputs and simultaneous removal by this
120 globally important marine N₂-fixer, as well as a broader characterization of the utilization of
121 methylated amines like TMA by biogeochemically-critical marine microbes.

122 **Results and Discussion**

123 *Nutrient-limited physiology under increased CO₂*

124 A comprehensive depiction of the experimental design can be found in Fig. S1, and
125 proteomic results and their implications for nutrient limitation theory are presented in Walworth
126 et al. 2016 (5). Here, we focus on steady-state, transcriptional/translational changes to nitrogen
127 source-sink metabolism as they relate to other biogeochemically-important pathways. Briefly
128 summarizing Fig. S1, a single IMS101 population, originally isolated from an individual
129 *Trichodesmium* colony (22), was split into low (380-selected) and high (750-selected) CO₂
130 treatments of six biological replicates each, and grown for ~7 years (~1,000 and ~1,500
131 generations for 380- and 750-selected, respectively). Semi-continuous culturing methods were
132 used in a modified trace metal-clean Aquil medium (devoid of ammonia or other fixed nitrogen)
133 containing 25 µM EDTA, standard vitamins and trace metals, with 250 nM Fe and 10 µM
134 phosphate (PO₄³⁻). Next, Fe/P co-limited treatments were generated by sub-culturing three
135 biological replicates from each CO₂ treatment and incubating them in the aforementioned media
136 except with co-limiting levels of Fe (10 nM) and PO₄³⁻ (0.25 µM) for >1 year. To then mimic

137 episodic pulses of Fe or P typically experienced by Fe/P co-limited microbes in the oligotrophic
138 ocean (3, 23, 24), either Fe or P was added at replete concentrations to subcultures of the Fe/P
139 co-limited cell lines to generate P and Fe limited lines at both CO₂ levels, respectively.
140 Following a two-month acclimation period to create steady-state conditions, the lines were
141 sampled for molecular analyses.

142 Growth and N₂ fixation rates were significantly increased under high CO₂ in both nutrient
143 replete (r750) and P-limited (750-P) conditions relative to low CO₂/nutrient replete (r380) and
144 low CO₂/P-limited (380-P) treatments, respectively (Fig. 1). Conversely, no growth rate
145 differences were observed in high CO₂/Fe-limited (750-Fe) and high CO₂/Fe/P-co-limited (750-
146 Fe/P) cell lines relative to their corresponding low CO₂/Fe-limited (380-Fe) and low CO₂/Fe/P-
147 co-limited (380-Fe/P) conditions, respectively. In a recent study, Hong et al. (2017)(9) observed
148 a significant decrease in growth and N₂-fixation rates in both replete (r750) and Fe-limited
149 conditions in high CO₂ (750-Fe) relative to their controls, unlike this study and a number of other
150 previous replete (3-6, 10, 25-28) and high CO₂/Fe-limited studies (5). Hong et al. (2017) (9)
151 attributed these discrepancies to ammonia contamination and metal toxicity in all other past
152 studies, although ammonia was below detection limit in our prepared Aquil media and EDTA
153 concentrations were at 25 µM to control for metal toxicity (29). One central difference in this
154 study and nearly all others relative to Hong et al. (2017) (9) is that *Trichodesmium* cell lines were
155 adapted (4-6) or acclimated (10, 26-28) to low pH as a product of increasing CO₂ partial pressure
156 on seawater carbonate chemistry similar to pH reductions *in situ*. This contrasts with artificially
157 controlling pH with short-term acid/base additions as in Hong et al. (2017), which may also
158 result in other unknown and uncontrolled effects to cell physiology. A second fundamental
159 difference is that our Fe-single limited treatments were generated from pulsing phosphorus into

160 7-year, high CO₂-adapted cell lines co-limited for iron and phosphorus for ~1 year, similar to
161 persistent co-limitation conditions observed in the oligotrophic ocean (23, 24).

162 Looking ahead, it is predicted that increasing CO₂ will impact ecosystems more rapidly
163 than increasing sea surface temperature (30), which in turn will affect the adaptive evolution of
164 marine microbes and their contribution to elemental cycling. Hence, following long-term (~7-
165 year) adaptation of IMS101 to high CO₂ (3, 5, 6), we investigated changes to IMS101 molecular
166 physiology and nitrogen acquisition after ~1-year-long exposure to Fe/P-co-limitation, followed
167 by additions of either Fe or P to create steady-state, Fe- and P-single limitation treatments.

168 *Variable nitrogen assimilation strategies under nutrient co-limitation in a future ocean*

169 Below we focus on the dynamics of global transcription and translation as they relate to
170 changing nitrogen metabolic strategies under intensifying nutrient (co)-limitation as a function of
171 high-CO₂ adaptation. A more in-depth discussion on other molecular changes in broad
172 biochemical pathways can be found in supplementary information. Genes in 380-Fe that were
173 differentially expressed (DE) when compared to r380, but not relative to 380-Fe/P, showed
174 significantly different transcript levels in both 380-Fe and 380-Fe/P, respectively, relative to r380
175 (Fig 2a, Dataset S1). This pool was enriched in Gene Ontogeny (GO) pathways involving
176 nitrogen fixation (downregulated), cytochrome-c oxidase activity (downregulated), copper ion
177 binding (downregulated), nitrate/nitrite transport (upregulated), respiration (downregulated),
178 glutamate synthase (upregulated), and amino acid transport (upregulated). These pathway
179 enrichments indicate a down-regulation of Fe-heavy N₂-fixing enzymes similar to other
180 findings(5, 31) in conjunction with the up-regulation of external nitrogen acquisition genes
181 targeting inorganic (e.g. nitrate; Fig. 3a) and/or possibly organic (e.g. amino acid transport)
182 sources (Dataset S1).

183 While the 750-Fe pool of DE transcripts relative to r380 was enriched in GO pathways
184 (Fig. S2) involved in nitrogen fixation (downregulated) and cytochrome-c oxidase activity
185 (downregulated), similar to 380-Fe relative to r380, genes involved in nitrate/nitrite transport
186 drastically reduced expression levels in 750-Fe (grey bar) and 750-Fe/P (blue bar) relative to
187 380-Fe (orange bar) and 380-Fe/P (green bar), respectively (Fig. 3). This massive transcriptional
188 reduction in inorganic nitrogen transport going from low to high CO₂ in Fe-limitation regardless
189 of P concentration also co-occurred with ~50% fewer genes being differentially expressed
190 overall in high CO₂/low Fe, including a considerable reduction of protein synthesis transcripts
191 (Fig. 2b, S2b; Dataset S1).

192 Interestingly, both transcript and protein abundances of a predicted TMA-oxidizing,
193 flavin-containing monooxygenase (FMO, Tery_3826) harboring the FMO-specific motif(32) and
194 a predicted transmembrane helix (per IMG annotation) sharply increased in 750-Fe (Figs. 2b,
195 3a), along with the flavin biosynthesis gene, *ribD* (Tery_1661; Dataset S1), relative to all other
196 treatments. In fact, the FMO gene was one of the most highly expressed transcripts detected in
197 the high CO₂, Fe-limited treatment. Furthermore, its general expression level is orders of
198 magnitude greater than other nitrogen acquisition transcripts across all treatments (Fig. 2b, 3b).
199 Transcripts of an annotated ammonia transporter (*amT1*; Tery_4477) remained unchanged across
200 treatments but was consistently expressed in the top ~6% of detected transcripts. Notably,
201 although 380-Fe and 750-Fe growth rates were similar, *ALDO* (Tery_1687; fructose-
202 biphosphate aldolase) transcript levels also drastically increased in 750-Fe along with the ferric
203 uptake regulator (Tery_3404, *fur*) and Fe-stress/photosynthesis antennae genes (Fig. 2b, Fig.
204 S2b).

205 Taken together, this global shift in transcript profiles in conjunction with the

206 downregulation of nitrate transport and the concurrent upregulation of FMO and *ribD* suggest
207 that high CO₂ intensifies iron limitation (5, 9) resulting in fundamental resource reallocation (e.g.
208 riboflavin) towards increased biosynthetic investment in FMO-mediated, iron-lean organic
209 nitrogen assimilation strategies. The large increase in FMO transcripts and proteins observed in
210 750-Fe suggests *Trichodesmium* preferentially scavenges TMA and possibly other organic
211 nitrogen and sulfur compounds under severe iron stress. Furthermore, FMO transcript and
212 protein abundances are in the top ~0.5% and ~10% of all detected gene transcripts and protein
213 products, respectively, irrespective of treatment, which indicates significant energetic investment
214 into persistent FMO biosynthesis. Conversely, nitrate transport transcripts are only in the top
215 ~50-70% of total transcripts, with no corresponding protein products detected in the proteome.
216 Upon calculating total mean expression of nitrogen acquisition transcripts across all treatments,
217 FMO was consistently expressed at significantly higher levels ($p < 0.0001$) than other nitrogen
218 acquisition genes (Fig. 3a), providing further evidence of persistent and enriched biosynthesis of
219 FMO. Taken together with the ammonia transporter expressed in the top 6% of overall
220 transcripts, these data support the notion that FMO-acquired compounds and ammonia are
221 preferred relative to nitrate acquisition as previously noted for ammonia(17). The TMA protein
222 was significantly more abundant in high-CO₂/low-Fe, low P, and Fe/P co-limitation relative to
223 r380, r750, and 380-Fe conditions, suggesting enhanced energetic investment into TMA enzyme
224 biosynthesis across various CO₂/nutrient-limited global change scenarios (Fig. 3c). It is
225 interesting that FMO transcript and protein levels considerably increased in 750-Fe but not 380-
226 Fe, although Fe-stress genes signaled iron limitation in both conditions. Strain IMS101 N₂-fixing
227 metabolism may be better adapted to low CO₂/low Fe due to prevalent Fe-limitation *in situ* (24)
228 thereby reducing the need to scavenge for nitrogen while molecular metabolic restructuring

229 induced by high CO₂/low Fe may require increased exogenous nitrogen for growth in an high-
230 CO₂ ocean. Since heterotrophs have been shown to grow on TMA as a sole C and N source (32),
231 *Trichodesmium* may utilize TMA for both C and N (33, 34). It was also recently shown that an
232 associated heterotrophic *Alteromonas macleodii* (*A. macleodii*) strain widely conserved in
233 *Trichodesmium* metagenomic consortia has the genetic potential to cleave DMSP to produce
234 DMS(35), which may be further oxidized by the *Trichodesmium* FMO, as DMS has been shown
235 to have nearly as high an affinity for FMO as that of TMA(32). Hence, TMA- and other FMO-
236 mediated assimilation may be a more general compensatory strategy utilized by *Trichodesmium*
237 for physiological maintenance in the face of fluctuating nutrients, which is evidenced by the
238 significant increase in FMO protein abundance across nutrient-limited treatments (Fig. 3a,
239 bottom panel).

240 N₂ fixation is strongly inhibited in the presence of 20 μM TMA, just as it is with 20 μM
241 nitrate (Fig. 3d). However, *Trichodesmium* growth rates are virtually unchanged in the presence
242 of 20 μM TMA relative to growth rates supported by N₂ fixation, comparable to results in the
243 presence of 20 μM nitrate, indicating that both fixed nitrogen sources can support growth as
244 efficiently as N₂. In contrast, the presence of 20 μM ammonia was toxic, and the cells were
245 unable to grow or fix N₂ at all (Fig. 3d). One recent study observed enigmatically high growth
246 and N₂ fixation rates in the presence of 20 μM ammonia (9), contrasting with all other previous
247 studies demonstrating drastic repression of N₂ fixation in exogenous ammonia concentrations
248 exceeding >10 μM (15, 17, 36, 37).

249 Although Hong et al. (2017) (9) observed decreases in the PSI:PSII ratio in 750-Fe
250 conditions similar to this study (Fig. 4a) and others(5, 31, 38), they also observed increases in the
251 iron-rich NifH protein in high CO₂/Fe-limiting conditions (750-Fe), contrasting with our

252 observed decreases in multiple nitrogenase transcripts and protein subunits in this study (Fig. 4b)
253 and another *Trichodesmium* iron-limited proteome (31). Although Hong et al. (9) suggest more
254 NifH is necessary in 750-Fe due to decreased enzyme efficiency, we observe a contrasting trend
255 via a fundamental shift in nitrogen metabolic strategy, whereby iron-rich gene abundances (e.g.
256 PSI and *nif* subunits) along with nitrate transport transcripts are significantly reduced under
257 severe iron stress concomitantly with increases in TMA-scavenging FMO and riboflavin
258 biosynthesis gene expression (750-Fe; Fig. 4a; Fig. S2).

259 Among the various forms of available exogenous nitrogen (e.g. amino acids, nitrate,
260 TMA, ammonia), one possible reason FMO may be preferred is that it can oxidize both nitrogen-
261 and sulfur-containing compounds including TMA, which may also serve as potential organic
262 carbon sources, thereby enabling *Trichodesmium* to assimilate several macronutrients by
263 minimizing energetic investment. Additionally, since *Trichodesmium* is physically colonized by
264 a diverse microbial consortium (35, 39) and methylated amine compounds like TMA are
265 ubiquitous as end products of, for example, protein putrefaction (32), *Trichodesmium* may have
266 consistent access to organic nitrogen/carbon sources as a product of biochemical decomposition
267 of cellular components by members of its consortium. This contrasts with the lifestyles of other
268 planktonic, unicellular marine bacteria, which typically harbor much less abundant and diverse
269 consortia. When searching *Trichodesmium* consortia metatranscriptome sequences (35) for FMO
270 via BLASTP (40), no significant hits were observed containing the FMO-specific motif,
271 suggesting it may not be widespread or expressed highly in consortia.

272 Although FMO homologs have been detected across global ocean datasets including
273 within the genomes of the ubiquitous SAR11 clade (32), only a handful of robust cyanobacterial
274 and bacterial homologs to IMS101 were detected with many of the remaining top high-scoring

275 pairs deriving from metazoans (Fig. S3; high-scoring pair $\geq 70\%$ of original *Trichodesmium*
276 FMO sequence length; e-value $\leq 10^{-5}$), yielding in an average percent identity of 27.9% (median
277 = 27.8%) over all pairs. We did detect the FMO genes in another *T. erythraeum* genome (strain
278 2175) and a *Trichodesmium* metagenome from hand-picked natural colonies (41) demonstrating
279 widespread retention and conservation of FMO. Interestingly, no homologs to other
280 biogeochemically-relevant marine cyanobacteria were detected. Taken together, FMO-mediated
281 scavenging may be ecologically advantageous for *Trichodesmium* in the oligotrophic ocean,
282 given its potentially persistent availability via biochemical degradation, and its relative scarcity
283 in its physically attached consortia as well as other sympatric cyanobacteria.

284 *Fe-single and Fe/P co-limited metabolism in the future ocean*

285 Our data suggest that interaction of limiting Fe with high CO₂ adaptation will intensify
286 iron stress in Fe/P co-limited molecular metabolism. For example, known P-stress genes (e.g.,
287 *phoX*, *sphX*, *phnG*), but not Fe-stress genes (e.g., *isiA*), were significantly upregulated in 380-
288 Fe/P, as compared to r380, thus suggesting that P-stress may be more prominent than Fe-stress
289 under low-CO₂/co-limiting conditions (Fig. 4; Fig. 5; Fig. S4; Dataset S2, S3). In fact, *isiA*
290 transcripts were significantly downregulated in both P-limited conditions irrespective of CO₂ as
291 well as in 380-Fe/P co-limitation (Fig. 4a). However, transcripts of Fe-stress genes, including
292 *isiA*, significantly increased in 750-Fe/P relative to 380-Fe/P accompanied by a significant
293 decrease in the PSI:PSII ratio, indicating iron stress in high CO₂/co-limitation (Fig. 4, Fig. 5).
294 Finally, this shift toward Fe stress is further evidenced by the high-confidence grouping of 750-
295 Fe with the 380- and 750-Fe/P co-limited treatments (AU-bootstrap p-value > 0.95) resulting
296 from hierarchical clustering of genes exclusively DE (i.e. transcriptional complement; Dataset

297 S3) in both 380- and 750-Fe/P (Fig. 6). Collectively, these data provide strong evidence for the
298 intensification of Fe stress on cellular metabolism upon interacting with high CO₂, regardless of
299 fluctuating P concentrations. Hence, iron-rich metabolic pathways that generate energy and fixed
300 nitrogen will likely be impacted as cells utilize alternative iron- and energy-conserving strategies
301 to acquire nutrients, with consequent reductions in new nitrogen inputs.

302 *P-single and Fe/P co-limited metabolism in the present and future ocean*

303 Upon adaptation to high CO₂, both 750-P growth and N₂ fixation increased relative to 380-P
304 (Fig. 1), while most 750-P-limited transcript levels remained statistically unchanged between
305 380-P and 750-P. This is evidenced by the much smaller number (n = 4) of DE genes between
306 380-P and 750-P as compared to those DE between 380-Fe and 750-Fe (n = 284; Fig. S5; Fig.
307 S6). Translation dominated the GO-enriched pathway pools for downregulated genes relative to
308 both r750 only and 750-Fe/P (Fig. S4; Fig. S6; Dataset S2) as in 380-P. It possible that increased
309 N₂ fixation rates of equivalently sized IMS101 cells under varying CO₂ conditions (e.g. r380 vs
310 r750; 380-P vs 750-P) may be driven by factors contributing to altered enzymatic rates rather
311 than by increases in enzyme abundance, as has been observed for temperature(42). This
312 possibility is supported by either unchanged or decreases in N₂ fixation transcripts and/or protein
313 abundances (e.g., *nifH*, *nifB*, *nifK*) in replete, 7-year high-CO₂ adapted IMS101 (r750) relative to
314 replete low CO₂ (r380), despite higher N₂ fixation rates in cells selected under elevated CO₂ (Fig.
315 4)(5). For some N₂ fixation genes, transcript increases were mirrored by increases in protein
316 abundances (e.g., *nifB*, Tery_4133; *nifK*, Tery_4138), though most remained unchanged in the
317 proteomic data (e.g., *nifH*, Tery_4136; *nifD*, Tery_4137). These trends suggest that different
318 nitrogenase genes may be independently regulated at the transcriptional level or have different
319 mRNA half-lives. Taken together, other regulatory mechanisms impacting enzymatic rates, but

not abundances, may be more generally associated with changes in CO₂-impacted physiology under P-limitation.

Fe/P co-limited transcription in the present and future ocean

Photosynthesis-related (e.g., Tery_0983, Tery_0998, Tery_5048, Tery_5049, Tery_0728), ferredoxin (e.g., Tery_0916, Tery_4539, Tery_5051), heme-containing (e.g., Tery_1714, Tery_0335), and N₂-fixing genes (Fig. 2; Fig. 4; Fig. 5; Fig. S7) were all downregulated in 380-Fe/P. This indicates a potential reduction and/or reallocation of Fe away from these pathways in the co-limited cells coinciding with reduced cell size (and therefore cellular elemental quotas), growth, and N₂ fixation relative to the replete conditions. Additionally, downregulation of GO-enriched pathways in 380-Fe/P involved in translational machinery and RNA binding (Fig. 5; Fig. S7) are consistent with observations in yeast and bacteria (i.e., stringent response) where proteins involved in cell growth and division (e.g., ribosomal proteins) have been observed to be downregulated in minimal (e.g. 380-Fe/P) vs rich (e.g. r380) medium (43, 44). Moreover, the upregulated 380-Fe/P (relative to r380) transcriptional complement also contained many genes involved in precursor metabolisms, potentially allowing for greater cellular plasticity and metabolic flexibility in low-nutrient regimes (5). Accordingly, we identified a set of upregulated proteins specific to 380-Fe/P co-limitation that included many involved in precursor metabolisms (i.e., isoprenoid biosynthesis); a finding consistent with prior observations in yeast maintained in minimal media(44). For example, 3-dehydroquinate synthase (Tery_2977, *aroB*) is upregulated solely in 380-Fe/P and is part of the shikimate pathway that produces chorismate, a precursor to aromatic amino acids including phenylalanine, tyrosine, and tryptophan (45)(Fig. S8).

Following 7 years of adaptation to high CO₂ and one year of growth at high CO₂ Fe/P co-

342 limitation conditions (750-Fe/P), transcript levels had shifted across broad metabolic pathways,
343 presumably orchestrating the maintenance of similar growth and N₂ fixation relative to 380-Fe/P
344 conditions (Fig. 5; Fig. S7). Of those genes that were exclusively DE during Fe/P co-limitation,
345 only ~5% (n = 26; Dataset S3) from the 380-Fe/P complement (n = 313) remained in the 750-
346 Fe/P complement (n = 174) (Dataset S3). In other words, these genes were either upregulated (n
347 = 15) or downregulated (n = 11) only in 380-Fe/P and 750-Fe/P co-limitation, relative to their
348 respective replete reference conditions (r380 and r750). Shared upregulated genes include the
349 universal stress global response regulator (Tery_2353, *uspA*), the aforementioned GTP-binding
350 gene (Tery_1904), and a carbohydrate selective porin gene (Tery_0838, *oprB*). The consistent
351 upregulation of these genes suggests that both 380- and 750-Fe/P co-limited cellular physiology
352 respond to environmental flux by consistently transcribing genes involved in general stress, bio-
353 timer regulation, and potential organic carbon uptake, as has been observed in other
354 cyanobacteria(33, 34). Shared downregulated genes include a 5',5'''-P₁,P₄-tetrphosphate
355 phosphorylase (Tery_0108, *ap₄A*), which has been implicated in bacterial stress responses and
356 gene regulation (46), and the mutator gene, *mutT* (Tery_4056), which has been demonstrated to
357 suppress transversion mutations (A•T to C•G) (47). Accordingly, *E. coli* Δ *mutT* deletion mutants
358 exhibited a 1000-fold increase in unidirectional A•T to C•G transversion frequencies. Other
359 studies have postulated that mutators can accelerate adaptive evolution under certain
360 circumstances via increased mutation rates(48). Hence, the significant reduction in transcription
361 of *mutT* in both long-term 380-Fe/P and 750-Fe/P treatments may help enable adaptive mutation
362 by possibly de-repressing transversion mutations in the face of low-nutrient, stress-inducing
363 environments.

364 Conclusions

365 Here, we show a marked shift in nitrogen metabolism going from low CO₂/Fe-limited to
366 high CO₂/Fe-limited regimes whereby iron-heavy pathways are significantly reduced, and
367 cellular investment is reallocated toward a predicted FMO-mediated organic nitrogen
368 scavenging, relative to acquisition pathways for inorganic nitrogen substrates. This fundamental
369 iron-saving strategy may also enable simultaneous assimilation of several other required
370 elements including C and S from methylated amines like TMA. Our data also suggest that
371 intensifying Fe-stress under high CO₂ may shift Fe/P co-limited metabolism into a more Fe-
372 limited metabolic state. This trend further highlights the need for iron-saving metabolic strategies
373 for nutrient limitation in a future high-CO₂ ocean. Additionally, N₂ fixation but not growth was
374 inhibited in the presence of TMA. If interactive global change factors intensify nutrient
375 limitation leading to enhanced organic nitrogen scavenging and reduced N₂ fixation by
376 *Trichodesmium*, future work must consider the relationship between N₂-fixation-mediated new-
377 nitrogen inputs and simultaneous removal from the fixed nitrogen pool. The shifting balance
378 between these two processes may have global implications for the role of *Trichodesmium* to the
379 future ocean biomes. Finally, transcript patterns in Fe/P co-limited metabolism also suggest
380 reductions in iron-heavy pathways in exchange for increases in precursor-related genes that may
381 aid cellular plasticity in response to varying nutrient concentrations. Although limitations in this
382 long-term experiment and others (49) include a steady-state environment lacking natural
383 variability as well as the use of a single strain of *Trichodesmium*, we believe our results
384 demonstrating molecular reallocations of nitrogen-acquisition and iron-sparing expression
385 provide robust indicators of potential *in situ* strategies some *Trichodesmium* populations may
386 employ while under co-varying nutrient limited regimes. We highlight consistent molecular
387 patterns in genes under Fe- and/or P-limitation while co-varying CO₂, which strengthens broad

388 trends outlined above. Future field work investigating co-limitation should aim to compare *in*
389 *situ* molecular patterns with those that we have identified in culture to try and help elucidate
390 universal indicators of co-limitation in the future ocean.

391 **Materials and Methods**

392 *Culturing Methods*

393 Details of nutrient-limited culturing methods can be found at Walworth et al. (2016)(5)
394 and in the supplementary materials and methods. For the growth experiment comparing TMA
395 with other N sources, IMS101 was grown in four N treatments: 1) N₂ 2) 20μM NaNO₃ 3) 20μM
396 TMA (Trimethylamine, C₃H₉N) 4) 20μM NH₄Cl. For all treatments, triplicate cultures were
397 maintained semi-continuously at 26°C under a light intensity of 150μmol photons m⁻²s⁻¹
398 irradiance (12L/12D cycle), cultures were diluted every other day, and 20μM N sources were
399 added after every dilution. Growth and nitrogen fixation rates were measured after 10
400 generations as described above and below.

401 Aquil medium was bubbled with 0.2μm-filtered prepared air/CO₂ mixtures (Praxair) and
402 in-line high-efficiency particulate air (HEPA) filters were employed to avoid Fe contamination
403 from particles in the gas tanks or lines. The pH was monitored daily with DIC being measured at
404 the final sampling. The acetylene reduction method was used to measure N₂ fixation rates of
405 *Trichodesmium* (4, 14, 25). Samples from each experimental triplicate (20 mL) were incubated
406 in gas-tight vials for 1 h after being injected with 2 mL acetylene in 23 mL of headspace. The
407 amount of ethylene produced was then analyzed by injecting a 200 μl aliquot of headspace gas
408 into a gas chromatograph (model: GC-8A, Shimadzu Scientific Instruments, Columbia, MD,
409 USA). An ethylene accumulation to N₂ fixation conversion ratio of 3 was used to calculate N₂
410 fixation rates. Upon steady state growth, *Trichodesmium* filament abundance and lengths were

411 measured in a 1mL-phytoplankton counting chamber using epifluorescence microscopy and
412 significant differences between nutrient conditions were calculated using two-way ANOVA
413 along with the Tukey test. For RNA sampling, cultures were swiftly and gently filtered onto 5
414 μm polycarbonate filters (Whatman) during the middle of the photoperiod, immediately flash
415 frozen, and stored in liquid nitrogen until RNA extraction.

416 *RNA isolation and extraction for Illumina Sequencing*

417 Samples for RNA were taken concomitantly with proteome samples in Walworth et al.
418 2016 (5) during the middle of the photoperiod for each replicate. Briefly, cells were swiftly and
419 gently filtered at 11 a.m. onto 5 μm polycarbonate filters (Whatman), immediately flash frozen,
420 and stored in liquid nitrogen until RNA extraction. RNA was extracted from 2 randomly chosen
421 biological replicates per treatment using the Ambion MirVana miRNA Isolation Kit (Thermo
422 Fisher Scientific) in an RNase free environment according to the manufacturer's instructions
423 followed by two incubations with Ambion's Turbo DNA-free kit to degrade trace amounts of
424 DNA. RNA was then submitted to the UC San Diego Institute for Genomic Medicine (IGM)
425 core for library preparation and sequencing (<http://igm.ucsd.edu/genomics/services.shtml>).
426 Briefly, rRNA removal and library construction was done with the Ribo-Zero rRNA Removal
427 Kit (Illumina) and TruSeq Stranded RNA Library Prep Kit (Illumina), respectively, and
428 multiplexed libraries were sequenced using the Illumina Hi-Seq yielding single-end 50 base pair
429 read libraries. Raw fastq files have been deposited in NCBI's Gene Expression Omnibus (50) and
430 are accessible through GEO Series accession number GSE94951. All protein spectral data used
431 in the above analyses can be found in Supplementary Data 4.

432 *Expression analysis*

433 Differential expression was done as previously described (6) and detailed methods can be
434 found in the supplementary materials and methods.

435 *Gene Ontology (GO) enrichment analysis*

436 As in Walworth et al. 2016 (6), Gene Ontology (GO) annotations for *Trichodesmium*
437 were downloaded from the Genome2D web server
438 (<http://pepper.molgenrug.nl/index.php/bacterial-genomes>). Next, the “phyper” function in “R” (R
439 Core Team 2014) was used to test for significant enrichment of GO categories among the
440 treatments and p-values were corrected with the Benjamin and Hochberg method(51) using the
441 “p.adjust” function ($p \leq 0.1$). Finally, genes in enriched GO categories were manually checked.

442 *Phylogenetic analysis*

443 FMO sequences for *T. erythraeum* strains IMS101 and 2175 were taken from the
444 Integrated Microbial Genomes (IMG) website (<https://img.jgi.doe.gov/>), and *Trichodesmium*
445 environmental metagenomic sequence data was downloaded from Walworth et al. 2015 (41).
446 The BLASTP algorithm was used to search sequences against the RefSeq protein database (52)
447 in which all high-scoring pairs were retained if the aligned portion spanned >70% of the original
448 query length with an evalue $< 10^{-5}$. Sequences were then aligned with MUSCLE v3.8.31 with
449 default settings(53), and spurious sequences and poorly aligned regions were removed with
450 trimAl 1.2rev59 (54). RAxML (55) was used for all maximum likelihood phylogenetic analyses
451 with the following settings: -f a -p 12345 -m PROTCATLG -N 100 -x 12345.

452 **Declarations**

453 *Availability of data and materials*

454 All RNA-Seq data used in this study have been deposited as raw fastq files in NCBI's Gene
455 Expression Omnibus (50) and are accessible through GEO Series accession number GSE94951.

456 All protein spectral data used in the above analyses can be found in Walworth et al. 2016 (5) in
457 Supplementary Data 4 (DOI: 10.1038/ncomms12081). Physiological and proteome data are
458 archived through the U.S. National Science Foundation Biological and Chemical Oceanography
459 Data Management Office (<http://www.bco-dmo.org/dataset/649904>).
460

461 *Conflict of Interest*

462 The authors declare that they have no competing interests.

463 *Acknowledgements*

464 This work was supported by US National Science Foundation grants OCE-1260233, OCE
465 1260490, and OCE 1657757 to D.A.H., E.A.W., and F.-X.F.
466

467 *Author contributions*

468 F.-X.F., D.A.H., and E.A.W. designed research; N.G.W., M.D.L., X.C., and F.-X.F. performed
469 research; N.G.W., M.D.L., X.C., F.-X.F., D.A.H., M.A.S, and E.A.W. analyzed data; and
470 N.G.W., M.D.L., F.-X.F., D.A.H., M.A.S, and E.A.W. wrote the paper.
471

472 **References**

- 473 1. **Hutchins DA, Fu F.** 2017. Microorganisms and ocean global change. *Nature*
474 *Microbiology* **2**:1–11. doi: 10.1038/nmicrobiol.2017.58
- 475 2. **Arrigo KR.** 2005. Marine microorganisms and global nutrient cycles. *Nature* **437**:349–
476 355.
- 477 3. **Hutchins DA, Boyd PW.** 2016. Marine phytoplankton and the changing ocean iron cycle.
478 *Nat Clim Change* **6**:1072–1079.

- 479 4. **Hutchins DA, Walworth NG, Webb EA, Saito MA, Moran D, McIlvin MR, Gale J,**
480 **Fu F-X.** 2015. Irreversibly increased nitrogen fixation in *Trichodesmium* experimentally
481 adapted to elevated carbon dioxide. *Nat Commun* **6**. doi: 10.1038/ncomms9155
- 482 5. **Walworth NG, Fu F-X, Webb EA, Saito MA, Moran D, McIlvin MR, Lee MD,**
483 **Hutchins DA.** 2016. Mechanisms of increased *Trichodesmium* fitness under iron and
484 phosphorus co-limitation in the present and future ocean. *Nat Commun* **7**:12081.
- 485 6. **Walworth NG, Lee MD, Fu F-X, Hutchins DA, Webb EA.** 2016. Molecular and
486 physiological evidence of genetic assimilation to high CO₂ in the marine nitrogen fixer
487 *Trichodesmium*. *Proc Natl Acad Sci USA* 201605202–8.
- 488 7. **Garcia NS, Fu F, Sedwick PN, Hutchins DA.** 2015. Iron deficiency increases growth
489 and nitrogen-fixation rates of phosphorus-deficient marine cyanobacteria. *ISME J* **9**:238–
490 245.
- 491 8. **de Baar HJW.** 1994. von Liebig's law of the minimum and plankton ecology (1899–
492 1991). *Progress in Oceanography* **33**:347–386.
- 493 9. **Hong H, Shen R, Zhang F, Wen Z, Chang S, Wenfang L, Kranz SA, Luo Y-W, Kao**
494 **S-J, Morel FMM, Shi D.** 2017. The complex effects of ocean acidification on the
495 prominent N₂-fixing cyanobacterium *Trichodesmium*. *Science* 1–9. doi:
496 10.1126/science.aal2981
- 497 10. **Hutchins DA, Mulholland MR, Fu F-X.** 2009. Nutrient cycles and Marine Microbes in a
498 CO₂-Enriched Ocean. *Oceanography* **22**:128–145.
- 499 11. **Saito MA, Bertrand EM, Dutkiewicz S, Bulygin VV, Moran DM, Monteiro FM,**
500 **Follows MJ, Valois FW, Waterbury JB.** 2011. Iron conservation by reduction of
501 metalloenzyme inventories in the marine diazotroph *Crocospaera watsonii*. *Proc Natl*
502 *Acad Sci USA* **108**:2184–2189.
- 503 12. **Fu F-X, Mulholland MR, Garcia NS, Beck A, Bernhardt PW, Warner ME, Sañudo-**
504 **Wilhelmy SA, Hutchins DA.** 2008. Interactions between changing pCO₂, N₂ fixation, and
505 Fe limitation in the marine unicellular cyanobacterium *Crocospaera*. *Limnol Oceanogr*
506 **53**:2472–2484.
- 507 13. **Chappell PD, Webb EA.** 2010. A molecular assessment of the iron stress response in the
508 two phylogenetic clades of *Trichodesmium*. *Environ Microbiol* **12**:13–27.
- 509 14. **Mulholland MR, Capone DG.** 1999. Nitrogen fixation, uptake and metabolism in natural
510 and cultured populations of *Trichodesmium* spp. *Mar Ecol Prog Ser* **188**:33–49.
- 511 15. **Fu F-X, Bell PRF.** 2003. Factors affecting N₂ fixation by the cyanobacterium
512 *Trichodesmium* sp. GBRTRL101. *FEMS Microbiology Ecology* **45**:203–209.
- 513 16. **Moore CM, Mills MM, Arrigo KR, Berman-frank I, Bopp L, Boyd PW, Galbraith**
514 **ED, Geider RJ, Guieu C, Jaccard SL, Jickells TD, La Roche J, Lenton TM,**

- 515 **Mahowald NM, Marañón E, Marinov I, Moore JK, Nakatsuka T, Oschlies A, Saito**
516 **MA, Thingstad TF, Tsuda A, Ulloa O.** 2013. Processes and patterns of oceanic nutrient
517 limitation. *Nat Geosci* **6**:701–710.
- 518 17. **Post AF, Rihtman B, Wang Q.** 2012. Decoupling of ammonium regulation and *ntcA*
519 transcription in the diazotrophic marine cyanobacterium *Trichodesmium* sp. IMS101.
520 *ISME J* **6**:629–637.
- 521 18. **Benavides M, Berthelot H, Duhamel S, Raimbault P, Bonnet S.** 2017. Dissolved
522 organic matter uptake by *Trichodesmium* in the Southwest Pacific. *Sci Rep* **7**:41315.
- 523 19. **Oren A.** 1990. Formation and breakdown of glycine betaine and trimethylamine in
524 hypersaline environments. *Antonie van Leeuwenhoek* **58**:291–298.
- 525 20. **Van Neste A, Duce RA, Lee C.** 1987. Methylamines in the marine atmosphere.
526 *Geophysical Research Letters* **14**:711–714.
- 527 21. **Gibb SW, Hatton AD.** 2004. The occurrence and distribution of trimethylamine-N-oxide
528 in Antarctic coastal waters. *Marine Chemistry* **91**:65–75.
- 529 22. **Prufert-Bebout L, Paerl HW, Lassen C.** 1993. Growth, nitrogen fixation, and spectral
530 attenuation in cultivated *Trichodesmium* species. *Appl Environ Microbiol* **59**:1367–1375.
- 531 23. **Mills MM, Ridame C, Davey M, LaRoche J, Geider RJ.** 2004. Iron and phosphorus co-
532 limit nitrogen fixation in the eastern tropical North Atlantic. *Nature* **429**:292–294.
- 533 24. **Sohm JA, Webb EA, Capone DG.** 2011. Emerging patterns of marine nitrogen fixation.
534 *Nat Rev Micro* **9**:499–508.
- 535 25. **Hutchins DA, Fu F-X, Webb EA, Walworth N, Tagliabue A.** 2013. Taxon-specific
536 response of marine nitrogen fixers to elevated carbon dioxide concentrations. *Nat Geosci*
537 **6**:1–6. doi: 10.1038/ngeo1858
- 538 26. **Kranz SA, Levitan O, Richter K-U, Prásil O, Berman-Frank I, Rost B.** 2010.
539 Combined effects of CO₂ and light on the N₂-fixing cyanobacterium *Trichodesmium*
540 IMS101: physiological responses. *Plant Physiol* **154**:334–345.
- 541 27. **Levitan O, Kranz SA, Spungin D, Prásil O, Rost B, Berman-Frank I.** 2010. Combined
542 effects of CO₂ and light on the N₂-fixing cyanobacterium *Trichodesmium* IMS101: a
543 mechanistic view. *Plant Physiol* **154**:346–356.
- 544 28. **Eichner MJ, Klawonn I, Wilson ST, Littmann S, Whitehouse MJ, Church MJ,**
545 **Kuypers MM, Karl DM, Ploug H.** 2017. Chemical microenvironments and single-cell
546 carbon and nitrogen uptake in field-collected colonies of *Trichodesmium* under different
547 pCO₂. *ISME J* **62**:986.
- 548 29. **Hutchins DA, Fu F, Walworth NG, Lee MD, Saito MA, Webb EA.** 2017. Comment on
549 “The complex effects of ocean acidification on the prominent N₂-fixing cyanobacterium

- 550 *Trichodesmium*.” Science **357**:eaao0067–3.
- 551 30. **Boyd PW, Cornwall CE, Davison A, Doney SC, Fourquez M, Hurd CL, Lima ID,**
552 **McMinn A.** 2016. Biological responses to environmental heterogeneity under future
553 ocean conditions. *Global Change Biol* **22**:2633–2650.
- 554 31. **Snow JT, Polyviou D, Skipp P, Christmas NAM, Hitchcock A, Geider R, Moore CM,**
555 **Bibby TS.** 2015. Quantifying integrated proteomic responses to iron stress in the globally
556 important marine diazotroph *Trichodesmium*. *PLoS ONE* **10**:e0142626.
- 557 32. **Chen Y, Patel NA, Crombie A, Scrivens JH, Murrell JC.** 2011. Bacterial flavin-
558 containing monooxygenase is trimethylamine monooxygenase. *Proc Natl Acad Sci USA*
559 **108**:17791–17796.
- 560 33. **Stuart RK, Mayali X, Lee JZ, Everroad RC, Hwang M, Bebout BM, Weber PK,**
561 **Pett-Ridge J, Thelen MP.** 2016. Cyanobacterial reuse of extracellular organic carbon in
562 microbial mats. *ISME J* **10**:1240–1251.
- 563 34. **Francisco ÉC, Franco TT, Wagner R, Jacob-Lopes E.** 2014. Assessment of different
564 carbohydrates as exogenous carbon source in cultivation of cyanobacteria. *Bioprocess*
565 *Biosyst Eng* **37**:1497–1505.
- 566 35. **Lee MD, Walworth NG, McParland EL, Fu F-X, Mincer TJ, Levine NM, Hutchins**
567 **DA, Webb EA.** 2017. The *Trichodesmium* consortium: conserved heterotrophic co-
568 occurrence and genomic signatures of potential interactions. *ISME J*. doi:
569 10.1038/ismej.2017.49
- 570 36. **Mulholland MR, Ohki K, Capone DG.** 2001. Nutrient controls on nitrogen uptake and
571 metabolism by natural populations and cultures of *Trichodesmium* (Cyanobacteria)¹. *J*
572 *Phycol* **37**:1001–1009.
- 573 37. **Mulholland MR, Ohki K, Capone DG.** 1999. Nitrogen utilization and metabolism
574 relative to patterns of N₂ fixation in cultures of *Trichodesmium* NIBB1067. *J Phycol*
575 **35**:977–988.
- 576 38. **Shi D, Kranz SA, Kim J-M, Morel FMM.** 2012. Ocean acidification slows nitrogen
577 fixation and growth in the dominant diazotroph *Trichodesmium* under low-iron conditions.
578 *Proc Natl Acad Sci USA* **109**:E3094–100.
- 579 39. **Rouco M, Haley ST, Dyhrman ST.** 2016. Microbial diversity within the *Trichodesmium*
580 holobiont. *Environ Microbiol* **18**:5151–5160.
- 581 40. **Altschul S, Gish W, Miller W, Myers EW, Lipman DJ.** 1990. Basic Local Alignment
582 Search Tool. *J Mol Biol* **215**:403–410.
- 583 41. **Walworth N, Pfreundt U, Nelson WC, Mincer T, Heidelberg JF, Fu F, Waterbury**
584 **JB, Glavina del Rio T, Goodwin L, Kyrpides NC, Land ML, Woyke T, Hutchins DA,**
585 **Hess WR, Webb EA.** 2015. *Trichodesmium* genome maintains abundant, widespread

- 586 noncoding DNA in situ, despite oligotrophic lifestyle. *Proc Natl Acad Sci USA* **112**:4251–
587 4256.
- 588 42. **Toseland A, Daines SJ, Clark JR, Kirkham A, Strauss J, Uhlig C, Lenton TM,**
589 **Valentin K, Pearson GA, Moulton V, Mock T.** 2013. The impact of temperature on
590 marine phytoplankton resource allocation and metabolism. *Nat Clim Change* **3**:979–984.
- 591 43. **Carneiro S, Lourenço A, Ferreira EC, Rocha I.** 2011. Stringent response of
592 *Escherichia coli*: revisiting the bibliome using literature mining. *Microbial Informatics*
593 *and Experimentation* 2011 1:1 1:14.
- 594 44. **Newman JRS, Ghaemmamghami S, Ihmels J, Breslow DK, Noble M, DeRisi JL,**
595 **Weissman JS.** 2006. Single-cell proteomic analysis of *S. cerevisiae* reveals the
596 architecture of biological noise. *Nature* **441**:840–846.
- 597 45. **Herrmann KM.** 1995. The shikimate pathway: Early steps in the biosynthesis of aromatic
598 compounds. *Plant Cell* **7**:907–919.
- 599 46. **Hou W-T, Li W-Z, Chen Y, Jiang Y-L, Zhou C-Z.** 2013. Structures of yeast Apa2
600 reveal catalytic insights into a canonical Ap4A phosphorylase of the histidine Triad
601 superfamily. *J Mol Biol* **425**:2687–2698.
- 602 47. **Akiyama M, Maki H, Sekiguchi M, Horiuchi T.** 1989. A specific role of MutT protein:
603 to prevent dG.dA mispairing in DNA replication. *Proc Natl Acad Sci USA* **86**:3949–3952.
- 604 48. **Taddei F, Radman M, Maynard-Smith J, Toupance B.** 1997. Role of mutator alleles in
605 adaptive evolution. *Nature* **387**:700–702.
- 606 49. **Collins S, Rost B, Rynearson TA.** 2013. Evolutionary potential of marine phytoplankton
607 under ocean acidification. *Evol Appl* **7**:140–155.
- 608 50. **Edgar R, Domrachev M, Lash AE.** 2002. Gene Expression Omnibus: NCBI gene
609 expression and hybridization array data repository. *Nucleic Acids Res* **30**:207–210.
- 610 51. **Benjamini Y, Hochberg Y.** 1995. Controlling the false discovery rate: a practical and
611 powerful approach to multiple testing. *J R Stat Soc B* **57**:289–300.
- 612 52. **Tatusova T, Ciufu S, Federhen S, Fedorov B, McVeigh R, O'Neill K, Tolstoy I,**
613 **Zaslavsky L.** 2015. Update on RefSeq microbial genomes resources. *Nucleic Acids Res*
614 **43**: D599–D605.
- 615 53. **Edgar RC.** 2004. MUSCLE: multiple sequence alignment with high accuracy and high
616 throughput. *Nucleic Acids Res* **32**:1792–1797.
- 617 54. **Capella-Gutiérrez S, Silla-Martínez JM, Gabaldón T.** 2009. trimAl: a tool for
618 automated alignment trimming in large-scale phylogenetic analyses. *Bioinformatics*
619 **25**:1972–1973.

- 620 55. **Stamatakis A.** 2014. RAxML version 8: a tool for phylogenetic analysis and post-analysis
621 of large phylogenies. *Bioinformatics* **30**:1312–1313.

622

623

624

625

626

627

628

629

630

631

632

633

634

635

636

637

638

639

640

641

642

643

644

645

646 **Figures**

647 **Figure 1 Cell physiology** Cell-specific growth rates in day⁻¹ (top panel), N₂-fixation rates
648 (middle panel), and cell sizes (assessed using the proxy carbon content per filament length (pg
649 C/μm)) (bottom panel) are shown. Experimental conditions are labeled on the left side of all
650 plots and color coded by nutrients. Data are shown as means and standard errors (n = 6).
651 Different letters denote statistical significance.

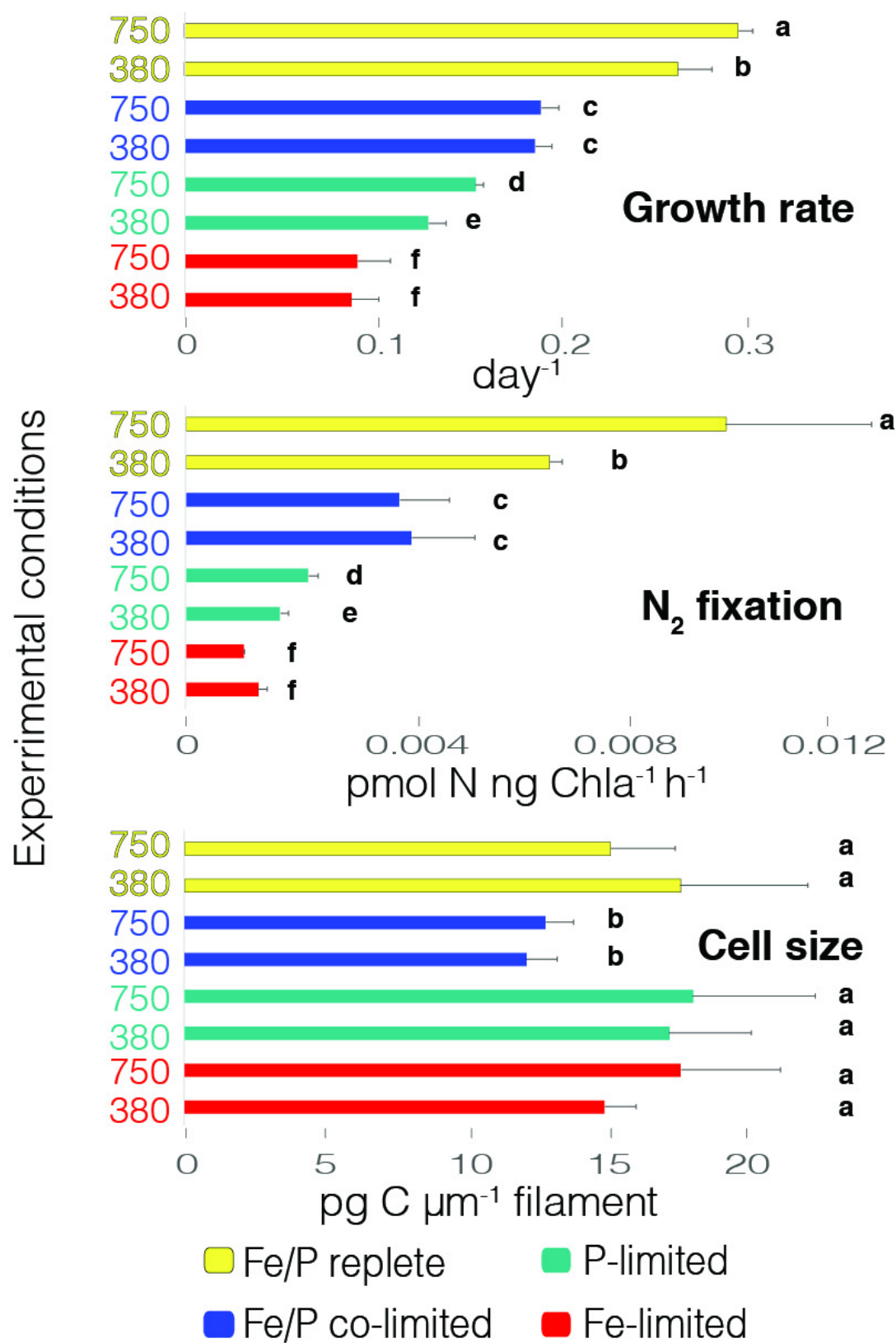
652
653 **Figure 2 Fe-limited vs Fe/P co-limited transcripts under 380 and 750 μatm CO₂** (a)
654 Scatterplot of 380-Fe differentially expressed (DE) genes relative to 380-Fe/P (blue) and 380-Fe
655 DE genes relative to both r380 and 380-Fe/P (magenta). Center diagonal shows a 1:1 line while
656 the other lines show 2:1 and 1:2, respectively. Insets are the same plot zoomed out to display
657 highly expressed genes. (b) Similarly, scatterplot of 750-Fe DE genes relative to either 750-Fe/P
658 (blue) or both r750 and 750-Fe/P (magenta). Select genes are labeled. The different colored
659 circles indicate genes within significantly enriched Gene Ontology (GO) pathways between the
660 two conditions.

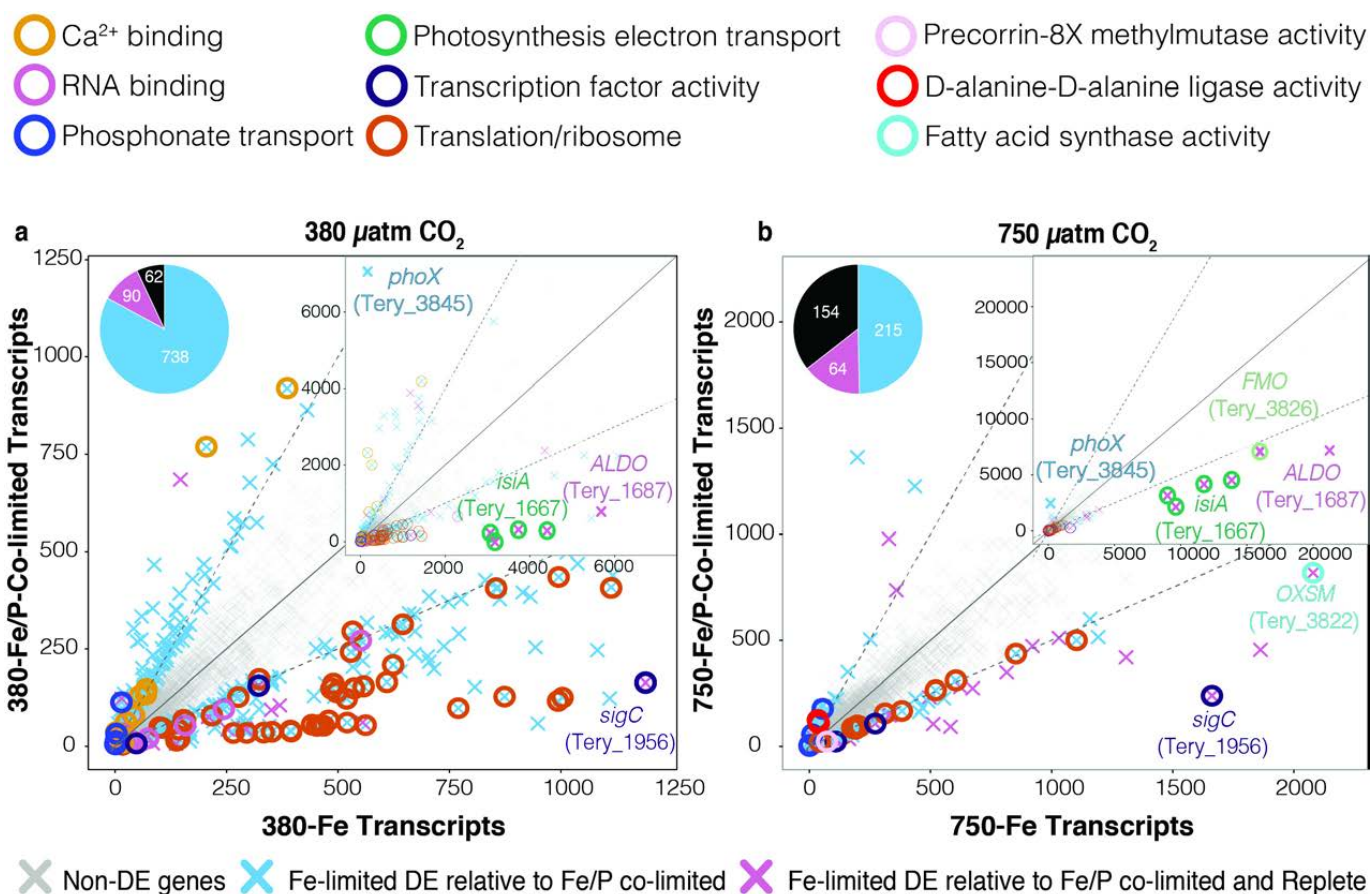
661
662 **Fig. 3 (a) Distributions of nitrogen acquisition transcripts across treatments, log₂ fold**
663 **changes of transcript and protein abundances per treatment, and (b) physiological data of**
664 **IMS101 grown on several nitrogen species.** (a) Top panel displays the distribution of
665 transcripts per gene across all treatments. Different letters signify significantly different mean
666 values. Middle panel shows log₂ fold changes of gene transcripts relative to the r380 condition
667 across experimental treatments. Bottom panel shows log₂ fold changes of normalized spectral
668 counts of the FMO gene relative to r380. Stars indicate statistical significance relative to r380.
669 (b) Growth and N₂ fixation rates are shown when IMS101 is grown without fixed nitrogen (N₂)
670 and in the presence of either NO₃, TMA, or NH₄ at 20 μm. Different letters signify significantly
671 different mean values.

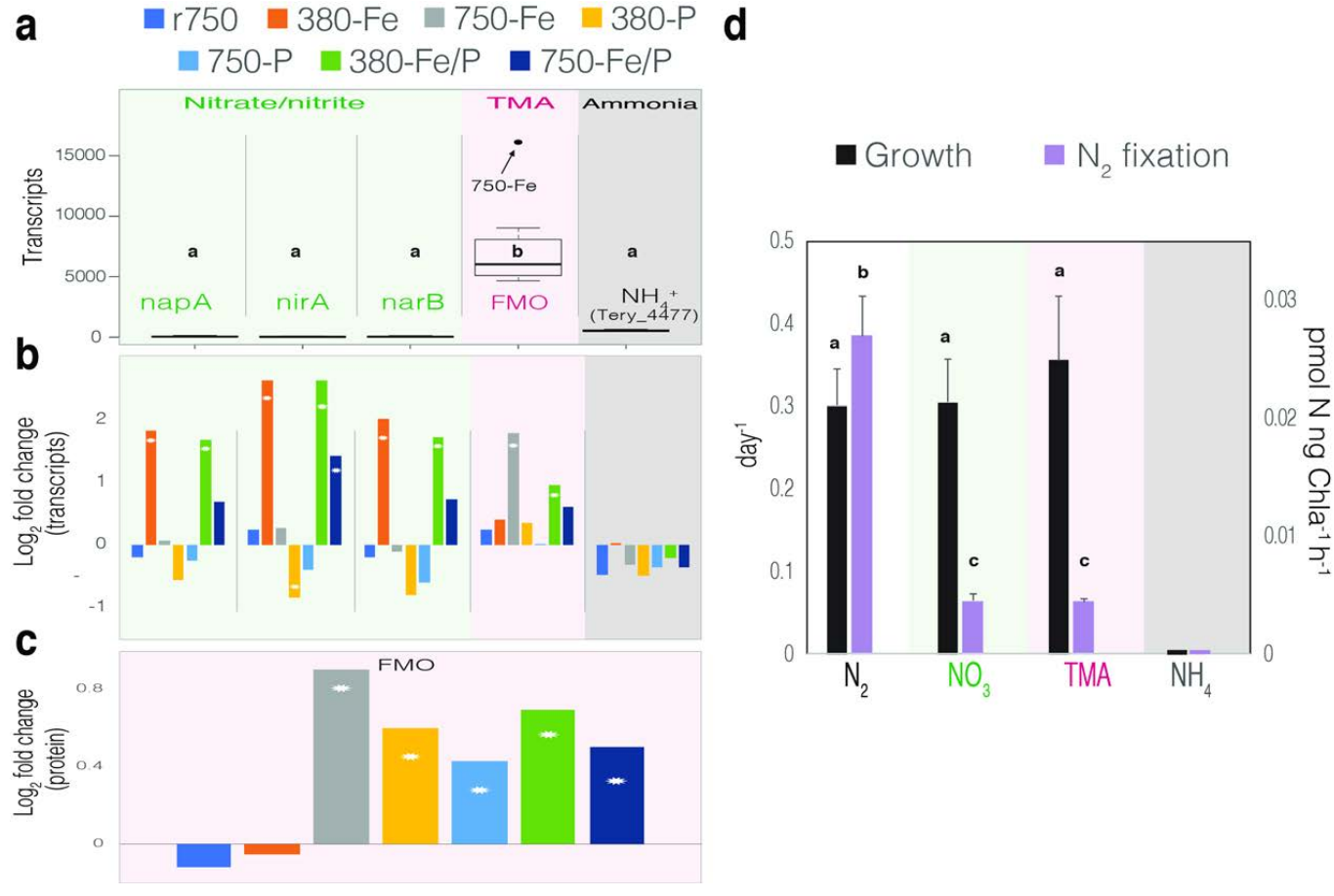
672
673 **Fig. 4 (a) Log₂ fold changes of normalized transcript and protein abundances of**
674 **photosystem genes and (b) genes from various pathways.** (a) Top panels shows log₂ fold
675 changes of gene transcripts relative to the r380 condition across experimental treatments. Bottom
676 panels shows log₂ fold changes of normalized spectral counts of the FMO gene relative to r380.

677
678 **Figure 5 Replete vs Fe/P co-limited transcripts under 380 and 750 μatm CO₂** (a) Scatterplot
679 of 380-Fe/P differentially expressed (DE) genes relative to r380 (tan) and 380-Fe/P DE genes
680 relative only r380 and no other 380-nutrient limitations (magenta). Center diagonal shows a 1:1
681 line while the other lines show 2:1 and 1:2, respectively. Insets are the same plot zoomed out to
682 display highly expressed genes. (b) Similarly, scatterplot of 750-Fe/P DE genes relative to r750
683 (tan) and 750-Fe/P relative only r750 and no other 750-nutrient limitations (magenta). Select
684 genes are labeled. The different colored circles indicate genes within significantly enriched Gene
685 Ontology (GO) pathways between the two conditions.

686
687 **Figure 6 Hierarchical clustering of 380- and 750-Fe/P gene transcript complements**
688 Hierarchical clustering of Bray-Curtis dissimilarities with multiscale bootstrap resampling
689 calculated from normalized transcripts of all DE genes in both 380-Fe/P and 750-Fe/P
690 complements. Values at nodes are approximately unbiased (AU) p-values. Boxes highlight high-
691 confidence clusters with AU p-values > 0.95.







Log2 Fold Change from r380

